Journal of Engineering Science and Technology
Vol. 17, No. 2 (2022) 1577 - 1588

EFFECT OF TEMPERATURE ON THE CHARACTERISTICS OF BETA-TRICALCIUM PHOSPHATE FOR USE AS BONE SUBSTITUTE MATERIAL

L. T. BANG[1,*], S. RAMESH[2,3], BUI DUC LONG[1], NGUYEN ANH SON[1], TRAN BAO TRUNG[4], S. SIVAKUMAR[5]

[1] School of Materials Science and Engineering, Hanoi University of Science and Technology, Hanoi, Vietnam
[2] Center of Advanced Manufacturing and Material Processing, Department of Mechanical Engineering, Faculty of Engineering, University of Malaya, 50603 Kuala Lumpur, Malaysia
[3] Mechanical Engineering Programme Area, Faculty of Engineering, Universiti Teknologi Brunei, Tungku Highway, Gadong BE1410, Brunei Darussalam
[4] Institute of Materials Science, Vietnam Academy of Science and Technology, Hanoi Vietnam
[5] School of Computer Science and Engineering, Taylor's University, 47500 Subang Jaya, Selangor, Malaysia
*Corresponding Author: bang.lethi@hust.edu.vn

Abstract

Beta tricalcium phosphate (β-TCP) has received great attention mainly because of its excellent biodegradability. However, synthesis of single phase β-TCP with controlled properties without affecting the biocompatibility of the ceramic is a challenge. The aim of this research was to synthesize bioresrobable and osteoconductive β-TCP for use as a bone substitute material and to evaluate the mechanical properties of the ceramic. In this work, a two-step heat treatment process was adopted. Initially, the material was heat-treated at 700 ºC, and subsequently sintered at different temperatures of 1000, 1100 and 1200 ºC. It was revealed that the stability of the β-TCP phase was disrupted when sintered at 1200 ºC with some formation of α-TCP phase. The diametral tensile strength of phase-pure β-TCP sample was found to be about 4.06 MPa and was found to decline in the presence of α-TCP phase. Biological cell study showed that the β-TCP sample is excellent as a substrate for cell attachment, proliferation, differentiation, and mineralization, thus demonstrating excellent biocompatibility. This study showed that the β-TCP exhibited great potential for use as bone substitute materials.

Keywords: Bone substitute, Calcium phosphate, Direct sintering, Tricalcium phosphate.

1. Introduction

Calcium phosphate bioceramics (CaP) have been widely investigated for the use as a bone graft in reconstruction of bone defects over the past 20 years, much of this work were focussed on improving the processing conditions, the use of dopants and subsequently controlling the sintering parameters to obtain an optimised CaP for a host of medical applications [1-10]. The most desirable property of CaP is their ability to form a bond with host bone which resulted in a strong interface between bone and implant [11, 12]. Among the calcium phosphates, sintered hydroxyapatite (HAp: $Ca_{10}(PO_4)_6(OH)_2$) and β-tricalcium phosphate (βTCP: $Ca_3(PO_4)_2$) have been widely studied because of its excellent tissue response and good osteoconductivity [13-18]. However, HAp is stable and will not be replaced by natural bone through osteoclasts resorption [19-22]. In contrast, due to its biodegradability nature, β-TCP can be replaced by newly formed hard tissues [23-25] when exposed in biological environment. Therefore, β-TCP facilitates the process of bone remodeling [26], which makes it an ideal material for clinical applications [25, 27].

Depending upon the processing technique, calcium phosphate bioceramics having various morphology and level of crystallinity could be obtained [5, 14, 16, 18]. Wet-chemical methods (precipitation, hydrothermal technique, and hydrolysis of other calcium phosphate) have been used to produce synthetic β-TCP powders due to its simplicity and capacity of yielding pure products at reasonable costs [28-31]. However, the incomplete reaction during precipitation has been reported to have an effect in altering the stoichiometry and formation of residual phases [27]. In addition, calcination of powders is always needed at high temperatures (typically up to 1200 ^oC) to remove organic components in the structure. On the other hand, the characteristics and mechanical properties of TCP produced by these methods depend upon reaction parameters such as temperature, stirring rate, reactant concentrations and pH. These must be carefully controlled in order to obtain a pure product.

In contrast, the solid-state reaction usually gives a well-crystallized product, and has also been used to synthesized β-TCP. By using this method, raw materials containing Ca^{2+} and PO_4^3, i.e., $CaCO_3$ and $CaHPO_4 \bullet 2H_2O$ were mixed and heated at a relative high temperature for long duration. However, the TCP and minor secondary phase of CaO maybe obtained due to the unreacted $CaCO_3$ during the solid-state reaction. Furthermore, it is also difficult to obtained solid and dense sample with adequate mechanical strength due to the evaporation CO_2 and H_2O during the heat treatment process. In addition, the sinterability also affects the mechanical strength i.e., the higher the bulk density, the higher the mechanical strength would be, and this would require the green body to be sintered at relatively high temperatures above 1000^oC. However, it is a challenge to retain the β-TCP phase when sintered at higher temperatures. To overcome this problem, one of the strategies have been to use sintering additives to promote densification at lower temperatures [32, 33].

The aim of this work was to promote the use of a simple but reliable synthesis method to produce phase pure β-TCP that exhibits excellent sinterability at lower temperatures and good mechanical characteristics for use as a bone substitute material. In this study, a two-step heat treatment was used. In addition, the biocompatibility nature of the produced β-TCP exposed to MC3T3-E1 preosteoblast cells was examined.

2. Methods and Materials

2.1. Materials synthesis and characterization

β-TCP block was prepared from mixing calcium carbonate ($CaCO_3$) with calcium hydrogen phosphate dihydrate (DCPD), both purchased from Wako, Japan. The Ca/P ratio was kept at 1.5 and the mixing was done in a planetary ball mill for 2 h at 200 rpm (Pulverisette 5, Germany) containing ethanol as the mixing medium. The slurry was filtered and dried in an oven for at 70 °C for 24 h. The dried powders were subsequently compacted at 50 MPa using a standard stainless steel mold and calcined at 700 °C. For sintering study, the calcined samples were crushed into powder, and green samples of diameter 8 mm and 4 mm thickness were compacted at 50 MPa. These green samples were sintered at various temperatures, i.e., 1000, 1100 and 1200 °C, using a ramp rate of 5 °C/min. and holding time of 5 h prior to cooling inside the furnace.

X-ray structural analysis of the formation of β-TCP block was characterized by powder X-ray diffraction (XRD, EMPYREAN, PANalytical, Netherlands) using counter-monochromatic CuKα radiation generated at 40 kV and 40 mA. The XRD data was collected over 2θ range of 20 to 60°. The morphology of the β-TCP block was observed using scanning electron microscope (SEM: S-3600N, Hitachi High Technologies Co., Tokyo, Japan) at an accelerating voltage of 10 kV. The SEM micrographs were used to determine the grain sizes of the ceramic. The resulting chemical functional groups were evaluated using a standard Fourier transform infrared spectroscopy (FTIR) as described elsewhere [34, 35].

The bulk density of sintered samples was obtained by the water immersion method based on Archimedes' principle. The hardness of the sintered samples was obtained using a Vickers diamond indenter (Mitutoyo AVK-C2, USA) by applying 0.1 Kgf on the polished surfaces [36]. Three sample of each sintering condition was evaluated, and the hardness was determined at ten different locations per sample to calculate the average value. The diametral tensile strength (DTS) was determined using a universal testing machine (Instron, USA) operating at a crosshead speed of 1 mm/min. In this experiment, five samples were tested for each sintering condition. The diameter-to-thickness ratio of 4:1 was used for all samples and the samples were compressed to failure and the DTS is calculated at the maximum load.

2.2. Cell culture

In this experiment, MC3T3-E1 osteoblast-like cells (Riken Cell Bank, Tokyo, Japan) were cultured in L-glutamine containing alpha-minimum essential media in the presences of 10 vol.% fetal bovine serum, 1 vol.% penicillin and 10 mg/mL streptomycin [10]. The cells were kept at 37 °C under 5% carbon dioxide in a humidified environment and every 2-days the medium was replaced. When the cells confluence, the adherent cells were passaged and harvested using 0.25% trypsin–EDTA [37]. Cells at passage 3 were used for culture on the sample surface which were sterilized by heating in a vacuum oven at 120 °C for 3 h. For each sample groups, the test was performed in quadruple (n=4).

2.2.1. Immunofluorescence staining and proliferation

MC3T3-E1 cells were cultured for 24 hours on the specimens using 24-well plates with initial density of 10,000 cell/well. The cultured sample was then

washed 3 times using PBS, and subsequently treated with 4% paraformaldehyde for 10 minutes and 0.5% Triton X-100 for 5 minutes. The presences of vinculin were determined by staining the cells using monoclonal mouse anti-vinculin antibody and Alexa Flour 488 Goat anti-mouse IgG Antibody. The primary and secondary antibodies were both diluted 1:200 in PBS containing 1 mg/mL bovine serum albumin. The cells were also stained for actin using Acti-stain 555 phalloidin with Hoechst 33342 as a nuclear stain. After staining, the cells were washed 3 times with PBS prior to imaging using a fluorescence microscope (BZ-X710, Japan). A cell counting kit-8 (CCK-8, Japan) was used to determine the cell proliferation on the sample after an exposure period of 1 day and 5 days [10, 22].

2.2.2. Osteoblastic differentiation: Alkaline phosphatase activity

Alkaline phosphatase (ALP) activity was measured by LabAssayTM ALP (Wako, Japan) using p-nitrophenylphosphate as the substrate. Cells were seeded onto specimens at an initial density of 4×10^4 cells/ml and medium was changed every 2-days. After day 7 and day 21, the samples were rinsed twice with PBS and lysed with cell lysis buffer (Wako, Japan) for ~30 minutes. After centrifugation, 20 µl cell lysate supernatant was incubated with the assay buffer at 37 ºC for 15 minutes and the absorbance was spectrophotometrically measured at 405 nm. Total protein content was evaluated using Bio-Rad Protein Assay (Pierce Chemical Co., Illinois, USA). About 5-µl of the cell lysate supernatant was added to 100 µl assay buffer and agitated for 1 min. prior to measurement at 595 nm. The ALP activity was normalized by total protein content and expressed as unit/µg protein [10].

3. Results and Discussion

3.1. Material characterization

The XRD patterns of the samples after heat treatment at different temperatures are shown in Fig. 1. At temperatures of 1000 and 1100 ºC, all peaks were assigned to those of the XRD standard of β-TCP (ICDD 9-169). No secondary phase of impurity or the raw materials were detected. However, at 1200 ºC, small peaks of α-TCP were observed as shown in Fig. 1. This can be attributed to the transformation of β-TCP at this temperature since the phase transformation between α- and β-TCP is about 1125 ºC [27], although there have been reports that the transformation could also proceed at 1100 ºC [38]. However, it should be noted that both α- and β-TCP polymorphs are biocompatible and osteoconductive materials.

A typical SEM images of the sintered β-TCP sample are shown in Fig. 2. The β-TCP sample consists of spherical particles having diameter of about 0.89 µm at 1000 ºC. Upon increasing the heat treatment temperature, the particles become coarser with irregular shape. Further heating at 1200 ºC resulted in the formation of transgranular fracture on the surface of the sample. This may be due to the transformation of β-TCP to α-TCP. Similar morphology was also observed when β-TCP powder was synthesized by a wet chemical method and followed by calcination at 900 ºC [17, 29].

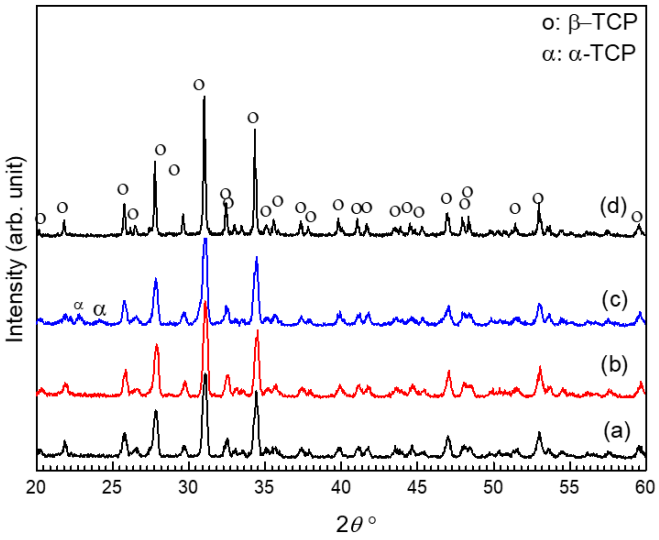

Fig. 1. XRD signatures of β-TCP samples sintered at different temperatures: (a) 1000 ºC, (b) 1100 ºC, (c) 1200 ºC, and (d) β-TCP standard (ICDD 9-169).

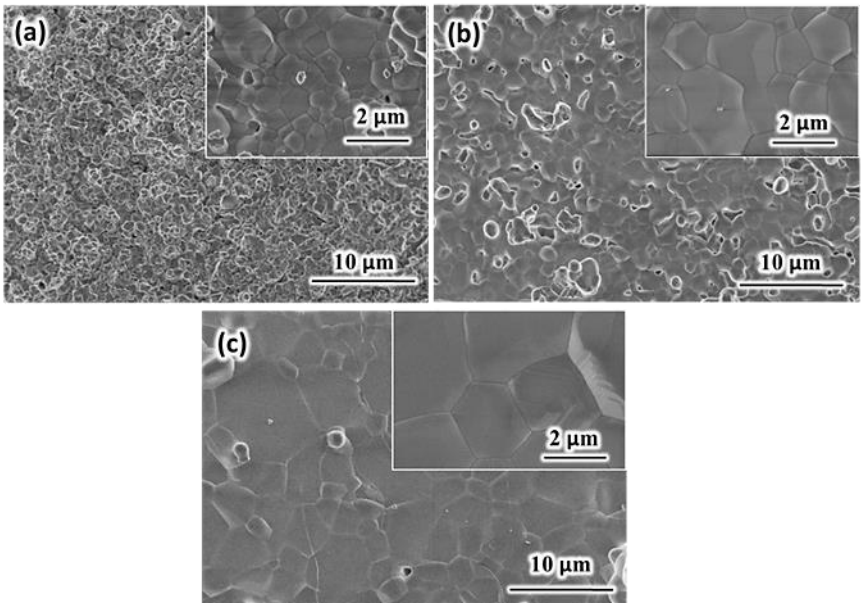

Fig. 2. SEM micrographs of samples sintered at (a) 1000 ºC, (b) 1100 ºC, (c) 1200 ºC (the inserted images are taken as higher magnification).

FTIR spectra of β-TCP samples sintered at different temperatures are shown in Fig. 3. Absorption bands assigned to the P-O vibration modes of the PO_4^{3-} group at 556, 604, and 1032–1100 cm^{-1}. A band at 970 cm^{-1} was assigned to v_1, symmetric stretching vibration of PO_4^{3-} group. A weak band about 942 cm^{-1} was assigned to the P-O(H) stretching in HPO_4^{2-} groups [31].

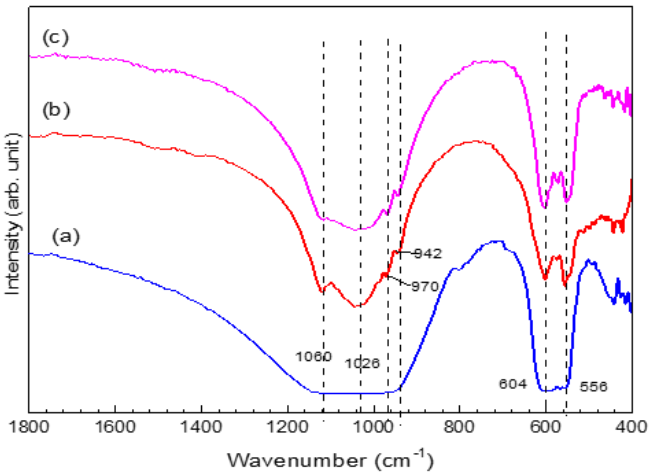

Fig. 3. FTIR spectra of β-TCP samples sintered at various temperatures: (a) 1000 °C, (b) 1100 °C, and (c) 1200 °C.

3.2. Mechanical properties

The sintered density was governed by the sintering temperature as shown in Fig 4. The results indicated that densification improved with increasing temperatures. The relative density of β-TCP at 1100 °C was about 81%.

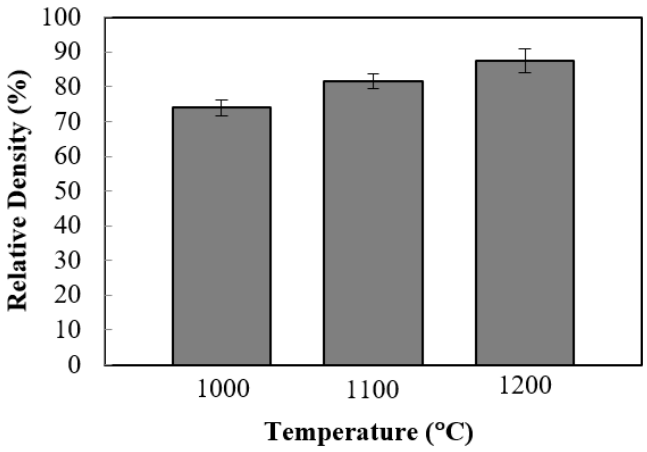

Fig. 4. Relative density of β-TCP samples sintered at various temperatures.

The variation in hardness and DTS of sintered samples is shown in Fig. 5(a) and Fig. 5(b), respectively. The differences that were observed in the sintered densities at low sintering temperature (1000-1100 °C) and the grain size at high temperature (1200 °C) are in good agreement with the hardness measurement. The general observation in Fig. 5(a) is that increasing the temperature from 1000 °C to 1200 °C resulted in an increased in hardness and this can be associated with an increase in their densities [29, 40].

On the other hand, the DTS, Fig. 5(b), was found to increase when the sintering temperature was increased from 1000 to 1100 ºC, corresponding to the single phase of β-TCP as shown in the XRD analysis. The highest DTS value of 4.06 MPa was recorded for the sample sintered at 1100 °C and this could be linked to the enhancement in densification as well as finer grain size [41]. On the other hand, sintering at 1200 ºC, the DTS value of the sample dramatically declined to the lowest value of 2.52 MPa. This behaviour could be associated to a combined effect of β-TCP grain coarsening, the presence of α-TCP that induced transgranular fracture (see Fig. 3) coupled with lower density.

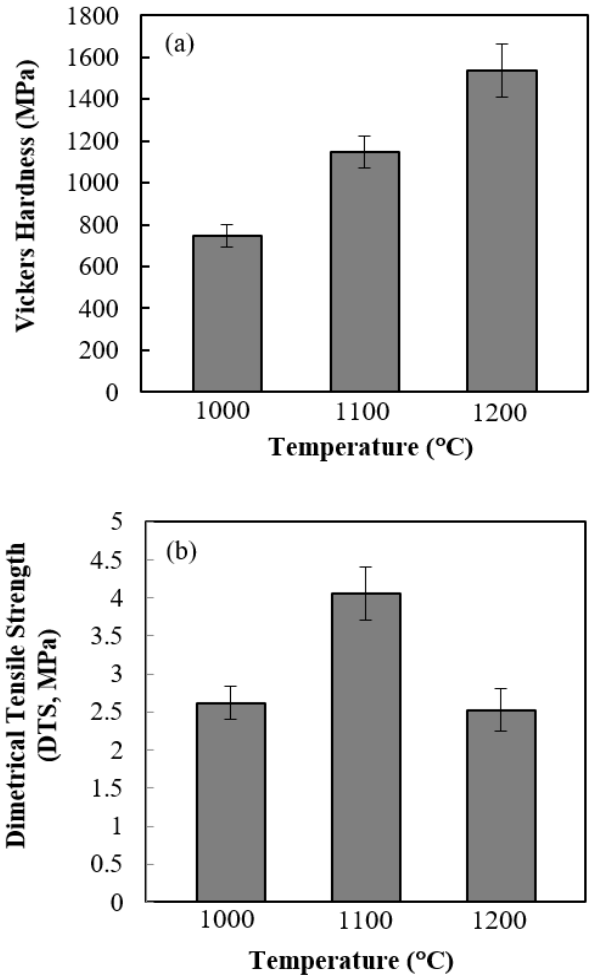

Fig. 5. The effect of sintering temperature on (a) Vickers hardness and (b) Diametrical Tensile Strength of TCP samples.

3.3. Early cell response using MC3T3-E1 cells

In this experiment, samples sintered at 1100 ºC was selected owing to their improved sintering characteristics and mechanical properties. The biocompatibility nature of the β-TCP was evaluated from the cell staining, cell proliferation,

differentiation, and mineralization. The immunofluorescence of cell morphology on the β-TCP substrates after culturing for 24 hours is shown in Fig. 6. Vinculin regulates various cell function including adhesion, migration, and apoptosis, and therefore, is important for determining the possibility of surface that can accommodate cell activities. As shown in Fig. 6, clear fluorescence of vinculin was observed indicating that cells had securely attached to the substrate, and subsequently increased cell spreading, altering cell morphology. As a result, the MC3T3-E1 cells exhibited a multilateral spindle shape with pseudopodia. The cell-cell contact has been shown to be essential for osteogenic differentiation of mesenchymal stem cells [42, 43]. The results of cell morphology suggest that the β-TCP is effective for promoting osteogenesis.

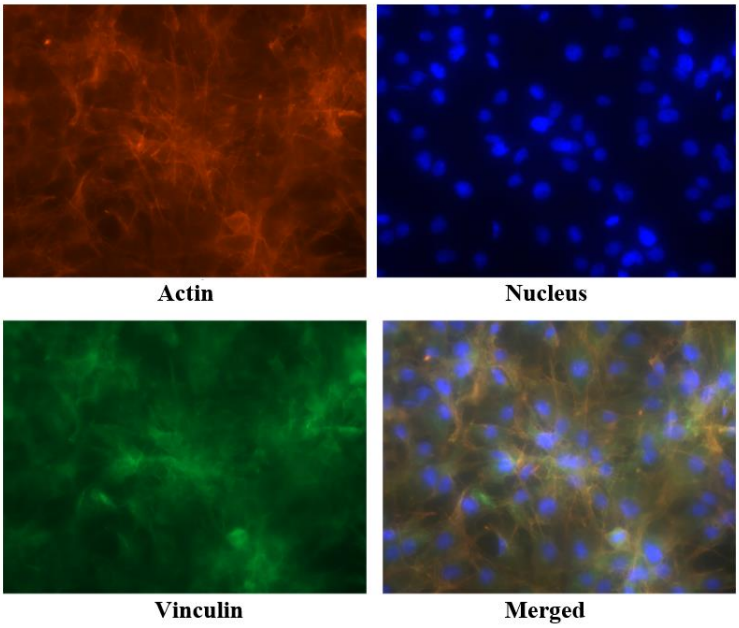

Fig. 6. Immunostaining of cells seeded on β-TCP.

The number of living cells and early osteoblast differentiation were further evaluated by a cell proliferation using CCK-8 assay, Fig. 7(a), and the alkaline phosphatase (ALP) activity, Fig. 7(b), respectively. For cell proliferation, the cell proliferation increased with the culture period indicating the possibility of improving long term biocompatibility. The increased in number of cells was evident after 5 days of culture as depicted in Fig. 7(a).

The number of cells observed on the substrates correlated with the enzymatic activity. The ALP activity of the sample surface significantly increased after the culture period. This demonstrated that the surface effectively induced the cells to differentiate toward osteoblastic phenotypes. The activity of alkaline phosphatase (ALP) was considered to indicate the presence of osteoblast cells that differentiated to mature osteoblasts, followed by the formation of new bone [44]. Nevertheless, quantification by immunostaining or a real-time PCR approach would be required for a better insight into bone formation.

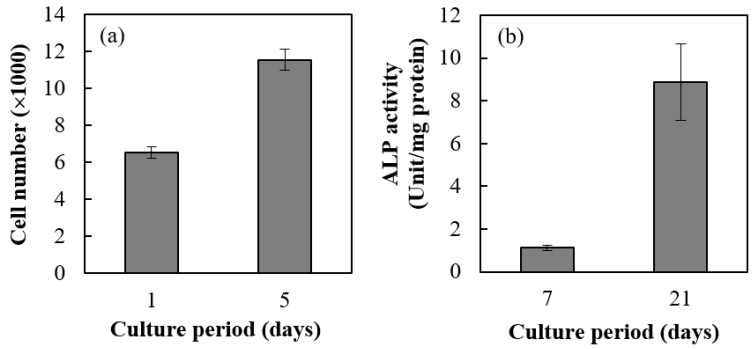

Fig. 7. Cell proliferation after 1 and 5 days (a) and relative ALP activity after 7 and 21 days of incubation (b) on β-TCP sample (*n*=4).

4. Conclusions

The production of phase pure β-tricalcium phosphate (β-TCP) has been achieved by the initial heat treatment at 700 ºC followed by sintering at 1100 ºC. The β-TCP phase stability was disrupted upon sintering at 1200 ºC with the formation of α-TCP phase. This phase transformation was accompanied by transgranular fracture on the sample surface. Although sintering at 1200 ºC resulted in improved hardness and density, the maximum diamentral tensile strength was obtained at 1100 ºC, in which the sintered body composed predominantly β-TCP phase. The biological cell responses study indicated that the β-TCP exhibited excellent biocompatibility for use as a promising candidate as bone substitute material.

Acknowledgement

This research was supported by Hanoi University of Science and Technology (HUST) under the grant number T2018-TT-206.

Abbreviations

ALP	Alkaline Phosphatase
$CaCO_3$	Calcium Carbonate
DTS	Diametral Tensile Strength
FTIR	Fourier Transform Infrared Spectroscopy
SEM	Scanning Electron Microscope
TCP	Tricalcium Phosphate
XRD	X-Ray Diffraction

References

1. Kutty, M.G.; and Ramesh, S. (2000). The effects of sintering temperature on the properties of hydroxyapatite. *Ceramics International*, 26(2), 221-230.
2. Sopyan, I.; Mel, M.; Ramesh, S.; and Khalid, K.A. (2007). Porous hydroxyapatite for artificial bone applications. *Science and Technology of Advanced Materials*, 8(1-2), 116-123.

3. Ooi, C.Y.; Hamdi, M.; and Ramesh, S. (2007). Properties of hydroxyapatite produced by annealing of bovine bone. *Ceramics International*, 33(7), 1171-1177.
4. Ramesh, S.; Tan, C.Y.; Bhaduri, S.B.; and Teng, W.D. (2007). Rapid densification of nanocrystalline hydroxyapatite for biomedical applications. Ceramics International, 33(7), 1363-1367.
5. Ramesh, S.; Natasha, A.N.; Tan, C.Y.; Bang, L.T.; Niakan, A.; Purbolaksono, J.; Hari Chandran; Ching, C.Y.; Ramesh, S.; and Teng, W.D. (2015). Characteristics and properties of hydoxyapatite derived by sol-gel and wet chemical precipitation methods. *Ceramics International*, 41(9), 10434-1044.
6. Ramesh, S.; Tan, C.Y.; Peralta, C.L.; and Teng, W.D. (2007). The effect of manganese oxide on the sinterability of hydroxyapatite. *Science and Technology of Advanced Materials*, 8(4), 257-263.
7. Tan, C.Y.; Yaghoubi, A.; Ramesh, S.; Adzila, S.; Purbolaksono, J.; Hassan, M.A.; and Kutty, M.G. (2013). Sintering and mechanical properties of MgO-doped nanocrystalline hydroxyapatite. *Ceramics International*, 39(8), 8979-8983.
8. Ramesh, S.; Tan, C.Y.; Yeo, W.H.; Tolouei, R.; Amiriyan, M.; Sopyan, I.; and Teng, W.D. (2011). Effects of bismuth oxide on the sinterability of hydroxyapatite. *Ceramics International*, 37(2), 599-606.
9. Ramesh, S.; Yaghoubi, A.; Sara Lee, K.Y.; Christopher Chin, K.M.; Purbolaksono, J.; Hamdi, M.; and Hassan, M.A. (2013). Nanocrystalline forsterite for biomedical applications: synthesis, microstructure and mechanical properties. *Journal of the Mechanical Behaviour of Biomedical Materials*, 25, 63-69.
10. Bang, L.T.; Ramesh, S.; Purbolaksono, J.; Ching, Y.C.; Long, B.D.; Hari Chandran; Ramesh, S.; and Othman, R. (2015). Effects of silicate and carbonate substitution on the properties of hydroxyapatite prepared by aqueous co- precipitation method. *Materials and Design*, 87, 788-796.
11. Habraken, W; Habibovic, P.; Epple, M; and Bohner, M. (2016). Calcium phosphates in biomedical applications: materials for the future?. *Materials Today*, 19(2), 69-87.
12. Yuan, H.; Barbieri, D.; Luo, X.; Van Blitterswijk, C.A.; and De Bruijn, J.D. (2017). Calcium phosphates and bone induction. *Comprehensive Biomaterials II*, 1, 333-349.
13. Vallet-Regí, M.; and Gonzalez-Calbet, J. (2004). Calcium phosphates as substitution of bone tissues. *Progress in Solid State Chemistry*, 32(1-2), 1-31.
14. Ramesh, S.; Tan, C.Y.; Hamdi, M.; Sopyan, I.; and Teng, W.D. (2007). The influence of Ca/P Ratio on the properties of hydroxyapatite bioceramic. *Proceedings of SPIE, vol.* 6423*: International Conference on Smart Materials and Nanotechnology in Engineering*. Edited by Shanyi Du, Jinsong Leng and Anand K. Asundi. SPIE Digital Library, USA, Paper No. 64233A.
15. Ruiz-Aguilar, C.; Olivares-Pinto, U.; Aguilar-Reyes, E.A.; López-Juárez, R.; and Alfonso, I. (2018). Characterization of β-tricalcium phosphate powders synthesized by sol–gel and mechanosynthesis. *Boletín de la Sociedad Española de Cerámica y Vidrio*, 57(5), 213-220.
16. Ramesh, S.; Tan, C.Y.; Tolouei, R.; Amiriyan, M.; Purbolaksono, J.; Sopyan, I.; and Teng, W.D. (2012). Sintering behaviour of hydroxyapatite prepared from different routes. *Materials and Design*, 34, 148-154.

17. Chaair, H.; Labjar, H.; and Britel, O. (2017). Synthesis of β-tricalcium phosphate. *Morphologie*, 101(334), 120-124.
18. Sopyan, I.; Ramesh, S.; and Hamdi, M. (2008). Synthesis of nano sized hydroxyapatite powder using sol-gel technique and its conversion to dense and porous bodies. *Indian Journal of Chemistry*, 47A, 1626-1631.
19. LeGeros, R.Z. (1993). Biodegradation and bioresorption of calcium phosphate ceramics. *Clin Mater*, 14(1), 65-88.
20. Sopyan, I.; Ramesh, S.; Nawawi, N.A.; Tampieri, A.; and Sprio, S. (2011). Effects of manganese doping on properties of sol-gel derived biphasic calcium phosphate ceramics. *Ceramics International*, 37(8), 3703-3715.
21. Hiromoto, S.; Itoh, S.; Noda, N.; Yamazaki, T.; Katayama, H.; and Akashi, T. (2020). Osteoclast and osteoblast responsive carbonate apatite coatings for biodegradable magnesium alloys. *Science and Technology of Advanced Materials*, 21(1), 346-358.
22. Bang, L.T.; Ramesh, S.; Purbolaksono, J.; Long, B.D.; Hari Chandran; Ramesh, S.; and Othman, R. (2015). Development of a bone substitute material based on alpha-tricalcium phosphate scaffold coated with carbonate apatite/poly-epsilon-caprolactone. *Biomedical Materials*, 10, 045011.
23. Eliaz, N.; and Metoki, N. (2017). Calcium phosphate bioceramics: a review of their history, structure, properties, coating technologies and biomedical applications. *Materials*, 10(4), 334.
24. Klein, P.A.T.; Patka, P.; and den Hollander, W. (1989). Macroporous calcium phosphate bioceramics in dog femora: a histological study of interface and biodegration. *Biomaterials*, 10(1), 59-62.
25. Wei, S; Ma, J.-X.; Xu, L.; Gu, X.-S.; and Ma X.-L (2020). Biodegradable materials for bone defect repair. *Military Medical Research*, 7(1): 54.
26. Mikai, A.; Ono, M.; Tosa, I.; Nguyen, H.T.T.; Hara, E.S.; Nosho, S.; Kimura-Ono, A.; Nawachi, K.; Takarada, T.; Kuboki, T.; and Oohashi, T. (2020). BMP-2/β-TCP local delivery for bone regeneration in MRONJ-like mouse model. *International Journal of Molecular Sciences*, 21(19), 7028.
27. Ghosh, R; and Sarkar, R. (2016). Synthesis and characterization of sintered beta-tricalcium phosphate: a comparative study on the effect of preparation route. *Materials Science and Engineering: C*, 67, 345-352.
28. Kang, K.-R; Piao, Z-G.; Kim, J.-S.; Cho, I.-A.; Yim, M.-J.; Kim, B.-H.; Oh, J.-S.; Son, J.; Kim, C.; Kim, D.; Lee, S-Y.; and Kim, S-G. (2017). Synthesis and characterization of β-tricalcium phosphate derived from haliotis sp. shells. *Implant dentistry*, 26(3), 378-387.
29. Kamalanathan, P.; Ramesh, S.; Bang, L.T.; Niakan, A.; Tan, C.Y.; Purbolaksono, J.; Hari Chandran; and Teng, W.D. (2014). Synthesis and sintering of hydroxyapatite derived from eggshells as a calcium precursor. *Ceramics International*, 40(10), Part B, 16349-16359.
30. Sanosh, K.P.; Cho, M.-C.; Balakrishnan, A.; Kim, T.N.; and Cho, S.-J. (2010). Sol-gel synthesis of pure nano sized β-tricalcium phosphate crystalline powders. *Current Applied Physics*, 10(1), 68-71.
31. Liu, L.; Wu, Y.; Xu, C.; Yu, S.; Wu, X.; and Dai, H. (2018). Synthesis, characterization of nano-β-tricalcium phosphate and the inhibition on hepatocellular carcinoma cells. *Journal of Nanomaterials*, 2018, Article ID 7083416.

32. Kalita, S.J.; Bhatt, H.A.; and Dhamne, A. (2006). $MgO–Na_2O–P_2O_5$-based sintering additives for tricalcium phosphate bioceramics. *Journal of the American Ceramic Society*, 89(3), 875-881.
33. Bhatt, H.; and Kalita, S. (2007). Influence of oxide-based sintering additives on densification and mechanical behavior of tricalcium phosphate (TCP). *Journal of Materials Science: Materials in Medicine*, 18, 883-893.
34. Duraisamy, N.; Numan, A.; Ramesh, K.; Choi, K.-H.; Ramesh, S.; and Ramesh, S. (2015). Investigation on structural and electrochemical properties of binder free nanostructured nickel oxide thin film. *Materials Letters*, 161, 694-697.
35. Safarzadeh, M.; Ramesh, S.; Tan, C.Y.; Hari Chandran; Ching, Y.C.; Mohd Noor, A.F.; Krishnasamy, S.; and Teng, W.D. (2020). Sintering behaviour of carbonated hydroxyapatite prepared at different carbonate and phosphate ratios. *Boletín de la Sociedad Española de Cerámica y Vidrio*, 59(2), 73-80.
36. Fairhurst, C. (1964). On the validity of the 'Brazilian' test for brittle materials. *International Journal of Rock Mechanics and Mining Sciences & Geomechanics Abstracts*, 1(4), 535-546.
37. Bang, L.T.; Tsuru, K.; Munar, M.; Ishikawa, K.; and Othman, R. (2013). Mechanical behavior and cell response of PCL coated α-TCP foam for cancellous-type bone replacement. *Ceramics International*, 39(5), 5631-5637.
38. Casas-Luna, M.; Horynová, M.; Tkachenko, S.; Klakurková, L.; Celko, L.; Diaz-de-la-Torre, S.; and Montufar, E.B. (2018). Chemical stability of tricalcium phosphate - iron composite during spark plasma sintering. *Journal of Composites Science*, 2(3), 51.
39. Van Landuyt, P.; Li, F.; Keustermans, J.P.; Streydio, J.M.; Delannay, F.; and Munting, E. (1995). The influence of high sintering temperatures on the mechanical properties of hydroxylapatite. *Journal of Materials Science: Materials in Medicine*, 6(1), 8-13.
40. Xu, J.L.; and Khor, K.A. (2007). Chemical analysis of silica doped hydroxyapatite biomaterials consolidated by a spark plasma sintering method. *Journal of Inorganic Biochemistry*, 101(2), 187-195.
41. Chen, B.; Zhang, T.; Zhang, J.; Lin, Q.; and Jiang, D. (2008). Microstructure and mechanical properties of hydroxyapatite obtained by gel-casting process. *Ceramics International*, 34(2), 359-364.
42. Sunarso; Toita, R.; Tsuru, K.; and Ishikawa, K. (2016). Immobilization of calcium and phosphate ions improves the osteoconductivity of titanium implants. *Materials Science and Engineering: C*, 68, 291-298.
43. Bang, T.L.; Ramesh, S.; Long, B.D.; Nguyen, A.S.; Munar, M.; and Shi, X. (2021). Effect of MgO addition on the sinterability, mechanical properties and biological cell activities of sintered silicon-substituted hydroxyapatite. *Journal of the Australian Ceramic Society*, 57, 857-868.
44. Shi, R.; Hayashi, K.; and Ishikawa, K. (2020). Rapid osseointegration bestowed by carbonate apatite coating of rough titanium. *Advanced Materials Interfaces*, 7(18), 2000636